Nuclear Instruments and Methods in Physics Research A 673 (2012) 64–72

Contents lists available at SciVerse ScienceDirect

Nuclear Instruments and Methods in Physics Research A

journal homepage: www.elsevier.com/locate/nima

Monte Carlo simulation of a single detector unit for the neutron detector array NEDA

G. Jaworski [a,b], M. Palacz [b,*], J. Nyberg [c], G. de Angelis [d], G. de France [e], A. Di Nitto [f], J. Egea [g,h], M.N. Erduran [i], S. Ertürk [j], E. Farnea [k], A. Gadea [h], V. González [g], A. Gottardo [l], T. Hüyük [h], J. Kownacki [b], A. Pipidis [d], B. Roeder [m], P.-A. Söderström [c], E. Sanchis [g], R. Tarnowski [b], A. Triossi [d], R. Wadsworth [n], J.J. Valiente Dobon [d]

[a] Faculty of Physics, Warsaw University of Technology, ul. Koszykowa 75, 00-662 Warszawa, Poland
[b] Heavy Ion Laboratory, University of Warsaw, ul. Pasteura 5A, PL 02-093 Warszawa, Poland
[c] Department of Physics and Astronomy, Uppsala University, Uppsala, Sweden
[d] INFN, Laboratori Nazionali di Legnaro, Legnaro, Italy
[e] GANIL, Caen, France
[f] INFN Sezione di Napoli, Napoli, Italy
[g] Department of Electronic Engineering, University of Valencia, Burjassot (Valencia), Spain
[h] IFIC-CSIC, University of Valencia, Valencia, Spain
[i] Faculty of Engineering and Natural Sciences, Istanbul Sabahattin Zaim University Istanbul, Turkey
[j] Nigde Universitesi, Fen-Edebiyat Falkültesi, Fizik Bölümü, Nigde, Turkey
[k] INFN Sezione di Padova, Padua, Italy
[l] Padova University, Padua, Italy
[m] LPC-Caen, ENSICAEN, IN2P3/CNRS et Université de Caen, Caen, France
[n] Department of Physics, University of York, York, United Kingdom

ARTICLE INFO

Article history:
Received 21 October 2011
Received in revised form
13 December 2011
Accepted 10 January 2012
Available online 20 January 2012

Keywords:
Monte Carlo simulation
BC501
BC501A
BC537
Liquid scintillator
Neutron detector
Geant4
NEDA

ABSTRACT

A study of the dimensions and performance of a single detector of the future neutron detector array NEDA was performed by means of Monte Carlo simulations, using GEANT4. Two different liquid scintillators were evaluated: the hydrogen based BC501A and the deuterated BC537. The efficiency and the probability that one neutron will trigger a signal in more than one detector were investigated as a function of the detector size. The simulations were validated comparing the results to experimental measurements performed with two existing neutron detectors, with different geometries, based on the liquid scintillator BC501.

1. Introduction

Modern arrays of germanium detectors are an ideal tool to perform in-beam γ ray spectroscopy investigations of exotic nuclei, far from the line of stability. In such studies the nuclei of interest are produced with very low cross-sections and aggregates of germanium detectors must be complemented with ancillary devices, which make accurate identification of the reaction products or reaction channels possible. In particular, when heavy-ion induced fusion-evaporation reactions are used to reach very neutron deficient nuclei, many reaction channels are open even at a moderate beam energy above the Coulomb barrier. The relative cross-section is largest for nuclei produced with the emission of a few protons. Channels with low proton multiplicity, α particle emission and, most important of all, emission of 2, 3, or more neutrons, have very small cross-sections but lead to the most exotic neutron deficient nuclei. Events of interest, for which γ rays should be analysed, can thus be selected by registering rare neutrons emitted from the compound nucleus, with additional conditions on detected protons and α particles.

* Corresponding author. Tel.: +48 22 5546206; fax: +48 22 6592714.
E-mail address: palacz@slcj.uw.edu.pl (M. Palacz).

0168-9002/$ - see front matter © 2012 Elsevier B.V. All rights reserved.
doi:10.1016/j.nima.2012.01.017

With the purpose of identifying neutron-evaporating reaction channels, large arrays of liquid scintillator detectors like the Neutron Wall [1,2] and the Neutron Shell [3] were constructed in the past and successfully used in many experiments, aiming at more and more neutron deficient nuclei, especially along and close to the $N=Z$ line, up to the region of the doubly magic ^{100}Sn. The existing neutron detection devices are rather well suited for the detection of single neutrons, achieving efficiencies of 20–30% in symmetric fusion-evaporation reactions (similar projectile and target masses). The detection and identification of two or more neutrons is more problematic. An important limitation of closely packed detector arrays, as the aforementioned ones, is the large probability that neutrons scatter between different detector units. This leads to an apparent increase of the number of detected neutrons and invalidates the selection of events with more than one emitted neutron. In order to achieve clean identification of events in which two or more real neutrons were detected, gates on time-of-flight difference and distance between active detectors have to be set [4,2]. This method allows to achieve a very good rejection of scattered neutrons, but it has a severe impact on the efficiency.

The γ rays are detected with similar intrinsic efficiency as neutrons in the liquid scintillator detectors. They have to be distinguished from neutrons, which is done by exploiting differences between the pulse shapes of the signals due to neutrons and γ rays and by time-of-flight measurements. A relatively good quality of the neutron–γ discrimination can be achieved: the residual probability to misinterpret a γ ray as a neutron is at the level of 0.5–0.1%. However, in experiments in which the average γ ray multiplicity is relatively large and the neutron emission is very rare, even such a low level of misinterpretation probability results in an unacceptably large number of wrongly identified events. This turns out to be critical if three or more neutrons should be detected and discriminated [2].

Work on the design of a new neutron detector array named NEDA (NEutron Detector Array) has recently been initiated. This work should lead to the construction of a more efficient neutron detection system than for example the Neutron Wall, with special emphasis on its ability to efficiently identify reactions in which several neutrons were emitted. In the present paper we report on a systematic Monte Carlo simulation study of a single detector module of NEDA, with the aim to maximise the neutron detection efficiency and to minimise neutron scattering to neighbouring detectors. The simulations were performed using the Geant4 package [5,6], which provide a full description of the interactions of radiation with matter as well as tools to implement complex detector geometries.

The Neutron Wall [1,2] and Neutron Shell [3] detector arrays use liquid scintillators of the type BC501A [7,8], which has the approximate chemical composition C_8H_{10}. For NEDA, the use of BC501A or possibly a deuterated scintillator, like BC537 (C_6D_6) [9], is considered. The deuterated scintillator is of interest because it may produce signals which are more correlated with the energy of the incident neutron, due to the anisotropic angular distribution of elastic scattering of neutrons on deuterons [10–13]. Such a property could make possible to distinguish single neutrons scattered between multiple detectors from the detection of multiple neutrons, by correlating the time-of-flight of the neutrons with the measurement of the energy deposited in the detectors.

The average energy of the neutrons in the laboratory system emitted in a typical fusion-evaporation reaction at the proton-rich side of the nuclidic chart is 2–3 MeV, with a tail extending up to about 10 MeV. An example of simulated neutron energy distributions, calculated using the evapOR code [14], can be found in Fig. 2 of Ref. [2]. In the present simulation study, we analyse the response of the detectors to monochromatic neutrons in the energy range 1–10 MeV. To validate the simulations (see Section 3) we have performed measurements with ^{252}Cf sources, which emit neutrons with an energy distribution [15] that is very similar to the one expected in the fusion-evaporation reactions of interest.

2. Geant4 and principles of neutron detection

The Geant4 package was the selected tool for the simulations of the NEDA array, due to its flexibility and the possibilities to include a large number of different materials and detector shapes. Moreover, the NEDA array will be used together with γ ray detector arrays, like AGATA [16], EXOGAM [17], GALILEO [18] and PARIS [19], and with charged particle detectors like DIAMANT [20], EUCLIDES [21], and CUP [22]. Geant4 models of most of these devices exist, and as consistent simulations of the complete detector setups are often necessary, the use of Geant4 for the NEDA simulations was imperative. The simulations which are presented here were performed in the framework of the AGATA simulation code [23], which greatly facilities combining all the above mentioned devices in one simulation.

Significant deficiencies of the neutron interaction model NeutronHP included in Geant4 versions earlier than 4.9.2 are, however, known. The results presented in this paper were obtained with Geant4 versions 4.9.2.p02 and 4.9.3 in which an attempt to correct the neutron interactions was made [24]. We decided anyway that the applicability of the model to our purpose should be verified. First, we have compared Geant4 generated angular distributions of neutrons elastically scattered on protons, deuterons and carbon nuclei to cross-sections of the ENDF VII data base [25], and the agreement was found to be good. Second, we have also checked the processes activated in Geant4 when neutrons interact in the scintillator liquid and analysed the spectra of the energy deposited in the scintillator by neutrons. This analysis is presented below. Note that earlier versions of the Geant4 NeutronHP model were not correctly reproducing the angular distributions. The list of possible processes and the energy spectra were also incorrect. Finally, two existing neutron detectors were irradiated with radioactive sources, and their measured performance was compared to the simulations, see Section 3.

Simulated histograms of the energy deposited by 10 MeV neutrons in a cylindrical scintillator volume are shown in Fig. 1. The processes responsible for the different structures in the histograms are indicated in the plots. In a hydrogen-based scintillator, the most important interaction of neutrons with an energy of a few MeV is elastic scattering on protons. This reaction gives rise to an isotropic distribution of the recoiling protons [26,27] in the centre-of-mass system, see also Ref. [28]. This leads to a flat proton energy distribution extending from zero to the energy of the incident neutron. A neutron, however, in a large volume detector usually undergoes a series of such interactions which sometimes leads to a deposit of the full energy of the neutron in the detector. This is the reason for the peak at 10 MeV in the spectra shown in Fig. 1.

At lower energies, the spectrum exhibits pronounced irregularities, which are due to interactions with ^{12}C. The sharp edge at 4.299 MeV is due to the endothermic reaction ^{12}C(n,α)^{9}Be ($Q=-5.701$ MeV). The two produced charged particles deposit their entire kinetic energy close to the interaction point. Another sharp edge is seen at 5.561 MeV in the spectra in Fig. 1. It is due to the deposit in the detector of the full energy of neutrons that have undergone inelastic scattering on ^{12}C, populating the first excited state at 4.439 MeV in ^{12}C that decays by the emission of a γ ray, which escapes from the detector. The trapezoidal shape between 7.26 MeV and 7.86 MeV indicates an incorrect functioning of

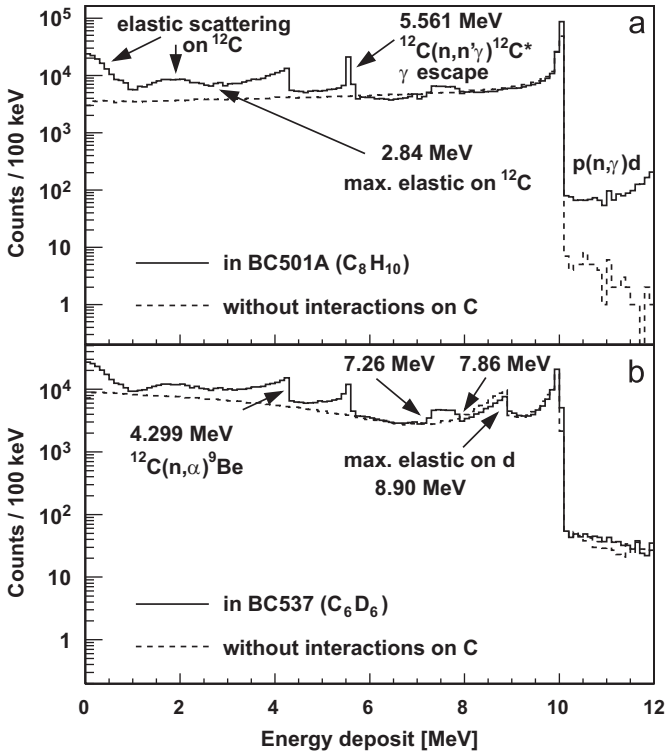

Fig. 1. Geant4 simulation of the energy deposited by 10 MeV neutrons in the two liquid scintillators (a) BC501A (C_8H_{10}) and (b) BC537 (C_6H_6). The detectors have a diameter of 12.7 cm (5 in.) and a length of 20 cm. The detector walls were not included in the simulations. The energy-deposit spectra for the hypothetical detector material consisting only of protons and deuterons (without carbon) are drawn with dashed lines.

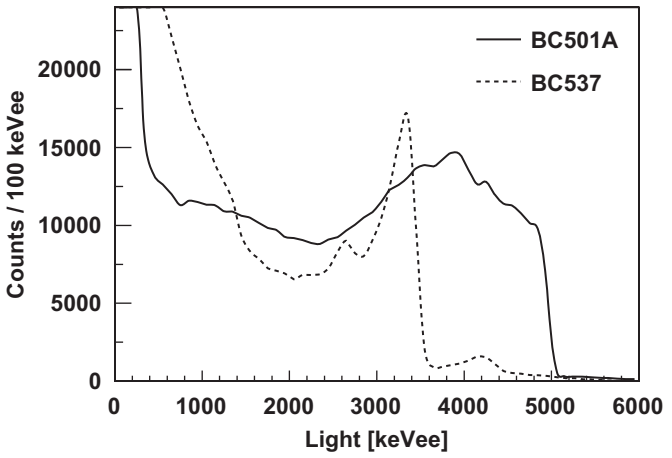

Fig. 2. Geant4 simulation: scintillator light output for 10 MeV neutrons in the detector of Fig. 1. An instrumental response function was not included in this calculation.

Geant4. The events leading to this shape originate from the reaction ^{12}C(n,α)^{9}Be, which never should lead to an energy deposit larger than 4.299 MeV. We have also noted that the reaction ^{12}C(n,n′)3α is missing in the list of Geant4 processes. The cross-section for this reaction is, however, not significant for neutron energies up to 10 MeV. The low-energy part of the spectrum, below 2.5 MeV, is dominated by elastic scattering on ^{12}C. Counts visible in Fig. 1a above the incident neutron energy of 10 MeV are due to exothermic capture on protons.

The spectrum of the energy deposit in the deuterated scintillator (Fig. 1b) resembles the one obtained for the proton based material, with the additional edge at 8.9 MeV which corresponds to the maximal single interaction energy transfer to a deuteron. Also, the spectrum slopes up at low energies, which reflects the anisotropy (forward and backward angles favoured) in scattering of neutrons on deuterons. Note that in the deuterated scintillator the relative number of events with full energy deposit is smaller than in the case of the proton based scintillator. In about 9% of events neutrons in the deuterated scintillator cause endothermic breakup of ^{2}H ($Q=-2.552$ MeV), and in 55% of these events energy is not properly conserved in Geant4. The Q-values calculated from kinetic energies of products of such reactions are distributed between -5 MeV and more than 10 MeV. Events of this kind, with the positive, erroneous Q-values, are responsible for counts visible above 10 MeV in Fig. 1b.

The neutron induced reaction products, or secondary particles produced in subsequent interactions, deposit energy in the scintillator and this energy is converted in our simulations to scintillation photons (light) using the parametrisation of Ref. [29]. Light may be produced by protons, deuterons, α particles, ^{9}Be and ^{12}C nuclei as well as by electrons and γ rays. The amount of light produced strongly depends on the type of particle moving in the scintillator. It is largest for electrons and γ rays and it is reduced for heavier particles. The unit 1 keVee (keV electron equivalent) is used for the light output (yield). It is the amount of light produced when an electron deposits an energy of 1 keV in the scintillator.

The light output for the scintillator cylinders used for Fig. 1 is shown in Fig. 2. The drastic difference between the shapes of the histograms of the produced light and of the deposited energy indicates the difficulties of obtaining direct information on the energy of the neutrons. Unlike the spectra of the deposited energy, the light histograms peak at zero energy. The majority of the events with very low light output are due to interactions on ^{12}C. Note that in a real measurement, the spectra are affected by the instrumental response function, which smears out the structures visible in Fig. 2, see Sections 3 and 7.

Experimentally, detectors count (register) neutrons (or γ rays) if the amplitude of the signal from the detector photomultiplier exceeds a certain level. The time of the detection is determined using for example a constant fraction discriminator. A similar procedure was applied in the simulation taking into account that each neutron usually interacts many times in the detector volume. In order to reproduce the experimental situation as close as possible, we first time sort the interactions, then sum them up incrementally. The "detection" time of the signal produced is defined as the time when the light produced in the detector exceeds the assumed threshold. In the following discussion, we use the term *significant interaction*, which refers to a series of interactions leading to a signal above threshold. A threshold of 50 keVee is assumed for most of the calculations presented in this work, except in Section 3 in which a larger threshold was used for a part of the data.

The analysis outlined above leads to the conclusion that the elastic scattering process on protons, deuterons and on ^{12}C is well reproduced in Geant4. Deficiencies of inelastic scattering on ^{12}C and ^{2}H were still identified. These deficiencies do not affect the results of the present work, as they contribute only to a small fraction of the neutron interaction cross-section in the interesting neutron energy range. In addition the amount of light produced in reactions on ^{12}C is much lower than in scattering on protons or deuterons.

3. Experimental validation of the simulation

In order to further validate the Geant4 simulations, experimental data were collected with two existing neutron detectors and the results were compared with the simulations. One of the

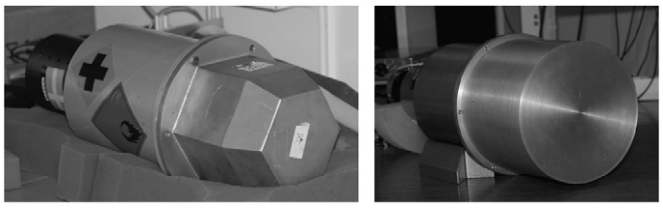

Fig. 3. Neutron detectors used in the test measurements: NORDBALL detector (left) and the cylindrical detector (right).

detectors was a NORDBALL neutron detector [30] which is made of a hexagonally shaped steel vessel, see Fig. 3, containing 3.9 l scintillation liquid of the type BC501 [7]. The other detector had a cylindrical shape with a diameter of 153 mm, length of 135 mm and contains 1.8 l of the same scintillator.

The detectors were irradiated by γ rays from the radioactive sources ^{137}Cs, ^{22}Na and ^{207}Bi, as well as by γ rays and neutrons from ^{252}Cf sources. Geant4 models were created for the two detectors and the simulations were run for both neutrons and γ rays. The content of the ^{250}Cf isotope in the neutron sources was taken into account in the data evaluation and simulations. The source used in the measurements with the NORDBALL detector was 35 years old, and at the time of the measurement it was emitting 6.0×10^3 and 4.3×10^3 neutrons per second, in the fission of ^{250}Cf and ^{252}Cf, respectively (compare Ref. [31]). The source used with the cylindrical detector was isotopically more pure, with 110 and 3.9×10^3 neutrons per second, respectively, emitted by the two isotopes. In the simulations it was assumed that the neutron energy distributions of both Cf isotopes were identical, and were given by the expression from Ref. [32]: $N(E)=\sqrt{E}\exp(-E/T)$, where $T=1.42$ MeV.

The measurements with the NORDBALL detector were performed at Uppsala University. The liquid was viewed through a glass window by a 14-stage, 5 in. diameter photomultiplier tube (PMT) of the type Philips XP2041. The high voltage used was -1.75 kV. The anode signal of the neutron detector was sent to an NDE-202 NIM electronic module [33]. This unit has a built-in circuit for neutron–γ discrimination based on the zero cross-over (ZCO) technique. It produces a TAC output signal corresponding to the time difference between the leading edge of the input signal, which is obtained from an internal constant fraction discriminator (CFD), and the ZCO time. The neutron–γ discrimination is done by setting a limit on the ZCO TAC amplitude. The NDE-202 unit also has a built-in charge-to-voltage-converter (QVC), which produces a signal proportional to the collected PMT charge. The ZCO TAC and the QVC signals were sent to a multichannel analyser system containing a 8192 channel peak-sensing ADC. The number of detected neutrons, which is needed for the determination of the neutron detection efficiency (see below), was obtained by integrating the number of counts in the neutron peak in the ZCO spectrum shown in Fig. 4a.

The measurements with the cylindrical 1.8 l detector took place at the Heavy Ion Laboratory in Warsaw. The PMT was of type XP4512B and the voltage used was -1.6 kV. The anode signal was digitised by a CAEN DT5720 12 bit, 250 MS/s digitiser connected to a laptop computer via a USB 2.0 cable. The readout of the data was triggered at time t_0, when the signal exceeded a threshold of an internal leading edge discriminator (LED) of the digitiser. The number of collected sampling points for each waveform was 64, including 17 samples acquired before t_0. The digitiser had to be protected against too large input signals. A LeCroy 428F fan-in–fan-out unit, which limits the amplitude to a maximum of -1.77 V, was therefore placed between the detector and the digitiser. The dead-time of the digitiser was estimated by

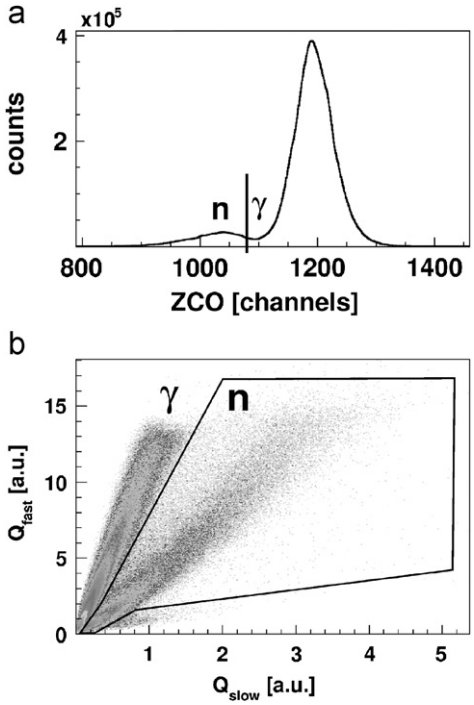

Fig. 4. Zero-cross-over time (ZCO) histogram (a) and two dimensional charge comparison plot (b) used for the neutron–γ discrimination in the Uppsala and Warsaw measurements, respectively. See text for the definition of Q_{fast} and Q_{slow}.

using a signal from an ORTEC 448 Research Pulser that was fed into one channel of the digitiser. The n–γ discrimination was performed off-line by using the charge comparison method [34,35], see Fig. 4b. The two charge values needed for the discrimination, Q_{fast} and Q_{slow}, were obtained by integrating signals in the time intervals (t_0,$t_{max}+20$ ns) and ($t_{max}+20$ ns, $t_{max}+60$ ns), respectively, where t_{max} is the time when the maximum of the signal height was detected. Neutron energy spectra were produced by integrating the area of the digitised waveforms.

The data collected with γ ray sources enabled calibration of the output signals in units of keVee. Background spectra were also measured and were subtracted from the spectra acquired with the sources, taking into account data taking times and the estimated dead times of the setups.

The resulting γ ray spectra obtained with the NORDBALL detector are shown in Fig. 5a–c. The broad peaks seen in the spectra are Compton edges of the respective γ rays. Simulations indicate that the actual Compton edge energy value corresponds to about 90% of the peak height to the right of the maximum of the peak. Based on such γ ray calibration points, the threshold (CFD or LED) values could be converted to keVee units, resulting in 115 keVee and 50 keVee for the Uppsala and Warsaw measurements, respectively. With known calibration and threshold values, the simulated spectra can be compared with the measured ones for both γ rays and neutrons, see Fig. 5. The light yield values (L) obtained in the simulation were randomised using a Gaussian distribution to account for the statistical effects of the light production, attenuation, photon to electron conversion and electron amplification. The standard deviation (σ) of this distribution was assumed to be proportional to $\sqrt{L}$ and the proportionality factor was adjusted to reproduce the width of the bump at Compton edge in the experimental ^{137}Cs spectrum, resulting in $\sigma=1.9\sqrt{L}$. The same Gaussian smearing function was used for the calculations presented in the following sections.

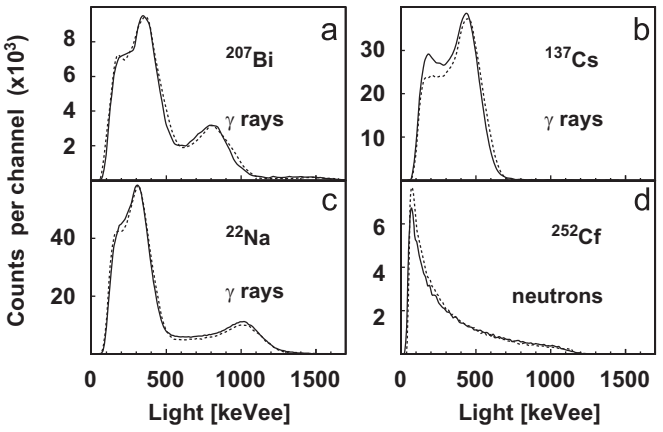

Fig. 5. Experimental (solid) and simulated (dotted line) γ ray spectra for the NORDBALL detector (a–c) and a neutron spectrum for the cylindrical detector (d). The simulated γ ray spectra shown in plots (a) and (c) are normalised to the maximum of the experimental distributions, while the ^{137}Cs γ ray and ^{252}Cf neutron histograms show true measured and simulated numbers of counts, corresponding to the source activity. The ^{207}Bi and ^{22}Na sources were placed at a distance of 20 cm from the front of the detector, while for ^{137}Cs and ^{252}Cf this distance was 50 and 5 cm, respectively.

Table 1
Comparison of the measured and simulated efficiency of the two neutron detectors. The intrinsic efficiency values were calculated as a ratio of the absolute numbers and the fraction of the solid angle covered by the front faces of the detectors. Distances between the sources and the front faces of the detectors are given in the first column. See the text for the discussion of the presented uncertainties.

	Efficiency (%) Absolute		Intrinsic	
Detector and radioactive source	Exp.	Sim.	Exp.	Sim.
NORDBALL:				
^{137}Cs γ rays, 50 cm	0.30(1)	0.285(1)	0.50(2)	0.476(7)
^{252}Cf neutrons, 51 cm	0.174(9)	0.241(2)	0.30(2)	0.419(4)
Cylindrical:				
^{252}Cf neutrons, 5 cm	6.1(3)	6.64(2)	0.283(14)	0.306(1)

The exact activities of the ^{207}Bi and ^{22}Na sources were not known, and thus the simulated spectra in plots (a) and (c) of Fig. 5 are normalised to the maximum of the experimental distributions. On the other hand, the ^{137}Cs and ^{252}Cf histograms show absolute numbers of counts obtained in the experiment and in the simulation for the same numbers of emitted γ rays and neutrons, taking into account the activities of the sources.

The shape of the simulated γ ray spectra agrees well with the measurements. The most notable difference is in the energy range 100–400 keVee in the ^{137}Cs histogram for which a larger number of counts were measured than what was obtained in the simulations. This effect could be attributed to γ rays scattered from the surrounding material into the detector, an effect that was not included in the simulations. We note, however, that it is not clear why a similar discrepancy is not seen in ^{22}Na and ^{207}Bi γ ray spectra in Fig. 5. Nevertheless, the absolute ^{137}Cs γ ray efficiency is rather well reproduced and is presented in Table 1.

In the low light part of the neutron spectrum the simulations give more counts than the measurement. One possible reason for this difference is that the neutron–γ discrimination works less well for signals with a small light yield, which leads to a loss of neutrons in the measurements [35]. Another explanation may be a problem of the threshold determination, for example due to a possible non-linearity of the energy calibration at low light yields. Note that the lowest γ ray calibration point was at 341 keV (Compton edge of the 511 keV γ ray). The threshold value was obtained by an extrapolation of the energy calibration to lower energies. The threshold position significantly influences the neutron detection efficiency as the neutron light distributions strongly peak at zero. It is also seen in Fig. 5 that all the simulated spectra are shifted to slightly higher energies compared to the measured spectra. This effect could be corrected for by changing the linear calibration coefficient by about 4%. The total neutron detection efficiency of the two detectors was calculated and compared with the simulations, see Table 1.

The experimental uncertainties given in Table 1 include statistical errors, errors of the data taking time determination (including dead time effects) and uncertainty of the source activities at the time of the measurement (which is the dominating uncertainty of the three mentioned here). The uncertainty of the neutron–γ discrimination for the ^{252}Cf sources is not taken into account. In case of the discrimination using the analogue ZCO value (the NORDBALL detector) this uncertainty is difficult to estimate, and likely leads to loosing a significant fraction of neutrons. This may explain the observed difference between the efficiency values obtained in the measurement and simulation for the ^{252}Cf neutrons in the NORDBALL detector. The agreement obtained for neutrons detected in the cylindrical detector is better. We anyway also in this case expect significant uncertainty of the neutron–γ discrimination, leading to an about 15% error bar on the number of the detected neutrons. Note that the imperfect neutron–γ discrimination may also lead to erroneous increase of the measured neutron detection efficiency, if some γ rays are misinterpreted as neutrons. We conclude that a satisfactory agreement between the measurement and simulation was obtained.

4. Optimum depth of the detector

In the attempt to find an optimum size of the NEDA detector modules, a systematic study was performed to determine the depth of the scintillator detector that is needed in order to register a significant interaction.

A pencil beam of monochromatic neutrons was shot into a scintillator cylinder with a 50 cm diameter and variable length. No detector walls were included in this simulation and the neutron detection efficiency was analysed as a function of the length of the cylinder. The efficiency to detect a neutron was defined as $\epsilon_n = N_{detected}/N_{emitted}$, where $N_{emitted}$ and $N_{detected}$ are the number of neutrons which were emitted and which created a significant interaction, respectively. The diameter was deliberately chosen to be rather large (50 cm), so that the detection probability depended only on the cylinder length and was not influenced by a limitation of the diameter. The results of this study are presented in Fig. 6.

The neutron detection probability as a function of the cylinder length reaches a constant value of about 80–95%, at a cylinder length from 20 to about 40 cm depending on the neutron energy and the type of the scintillator. A further increase of the detector length does not lead to a significant increase of the detection probability. Reaching an efficiency of 100% is not possible, because in some events neutrons lose energy in reactions which do not produce enough light to exceed the threshold.

We also analysed the depth distributions of the significant interactions. The results shown in Fig. 7 corroborate the above observations based on Fig. 6. The majority of the interactions take place within the first layers of the scintillator (depending on the neutron energy), but the tails of the depth distributions are large, thus the thickness of the scintillator necessary to detect almost all neutrons is also large (compare Fig. 6). The lowering of the mean

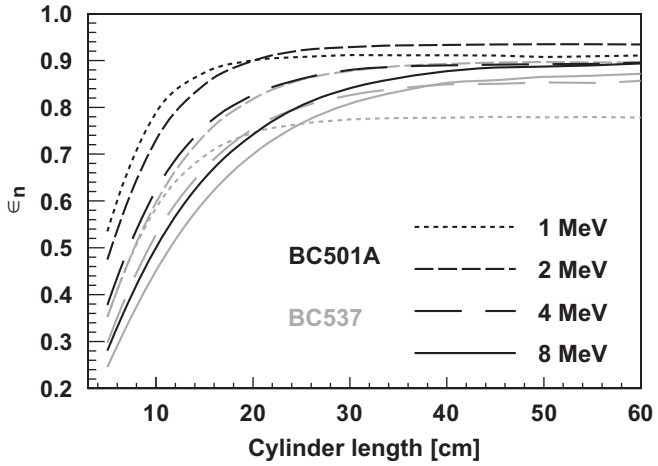

Fig. 6. Neutron detection efficiency (ϵ_n) as a function of the cylinder length for the two scintillators BC501A (black lines) and BC537 (grey lines) and for 1, 2, 4 and 8 MeV neutrons.

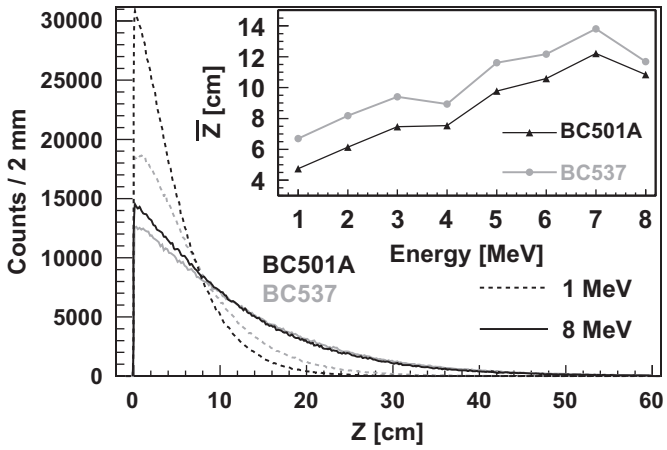

Fig. 7. Distributions of the depth of the significant interaction (Z) for two neutron energies and two scintillators, BC501A and BC537. The type of the scintillator is marked with black and grey lines for BC501A and BC537, respectively. The line pattern marks the neutron energy as shown in the legend. A total of 10^6 neutrons were simulated in each case. The insert shows the dependence of the mean significant interaction depth ($\overline{Z}$) on the neutron energy. Lines connecting the points in the insert are drawn only to guide an eye.

significant interaction depth at 4 MeV (see insert of Fig. 7) is attributed to the fact that elastic scattering on carbon becomes significant only at this energy (carbon nuclei moving in the scintillator are able to produce enough light). Thus, the total interaction cross-section increases at about 4 MeV. In turn, at 5.561 MeV the $^{12}C(n,\alpha)^9Be$ reaction channel opens, but the products of this reaction need another 2–3 MeV of kinetic energy to be detected, and therefore the significant interaction depths become smaller only at about 8 MeV.

We conclude that for most of the neutrons emitted in fusion-evaporation reactions, the maximum of the detection efficiency will be reached at a detector length of 20–30 cm. Increasing the detector length by another 10 or 20 cm would lead to slightly larger efficiency for the fastest neutrons. Two additional factors should, however, also be taken into account in determining the optimum length of the detector. The first one is the influence of the detector length on the probability that one neutron generates a signal in more than one detector. This is discussed further in Section 5. The second factor is the relation of the detector size to the quality of the neutron–γ discrimination. This effect was not studied in the present work, but the results presented in Ref. [36] indicate that the discrimination deteriorates for larger detectors.

5. Transverse size (diameter) of the detector

Neutrons undergo significant interactions mainly along the axis of their incoming direction. Distributions of the significant interaction with respect to this axis are shown in Fig. 8. After the first interaction, a scattered neutron may, however, produce another significant interaction, which is located far away from the initial axis, usually in another detector module. In order to study the distribution of such second significant interactions a setup was evaluated consisting of two coaxial detectors, an inner and an outer detector as shown in Fig. 9. Such a setup is a good representation of a detector module surrounded by a number of other modules, with unimportant geometrical details omitted.

A pencil beam of monochromatic neutrons was directed to the centre of the inner detector. The probability to register a significant interaction in the outer detector was evaluated for events in which the central detector fired, with the inner cylinder diameter varied within the range from 5 to 30 cm. The outer diameter of the setup was 1 m and detectors with two different lengths were used: 20 and 40 cm. The results are shown in Fig. 10. The plotted values are defined as $P_{1n\to 2n}=N_2/N_1$, where N_1 and N_2 are the number of neutrons which gave significant interactions in the inner cylinder and in both cylinders, respectively.

Fig. 10 indicates that $P_{1n\to 2n}$ is reduced rather slowly with the inner detector diameter. For any practical detector diameters the $P_{1n\to 2n}$ values will be large and if $P_{1n\to 2n}$ values below 1% are required (compare Ref. [2]) additional cleaning conditions of the interactions in two detectors cannot be avoided.

The $P_{1n\to 2n}$ values are significantly larger for longer detectors, for all energies and for both scintillators. The BC501A scintillator gives larger $P_{1n\to 2n}$ values than BC537 for the smallest diameters, but this relation inverts with the increase of the diameter, depending also on the energy of neutrons.

6. Times

A larger detector may in principle have worse time resolution. This may also impose an important limitation on the detector

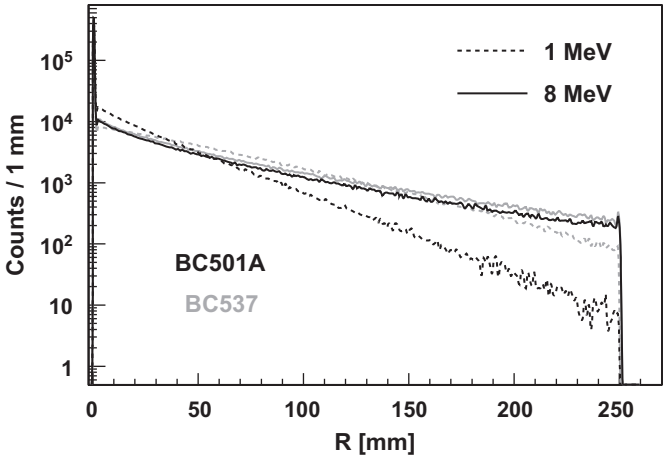

Fig. 8. Distribution of the distance (R) between the position of the first significant interaction and the axis of the incoming neutrons. The results of the simulations for two neutron energies (1 and 8 MeV) are shown with black and grey lines for the two scintillators, BC501A and BC537, respectively. A pencil beam of 10^6 neutrons were shot into the centre of the cylindrical detector in each of the presented cases.

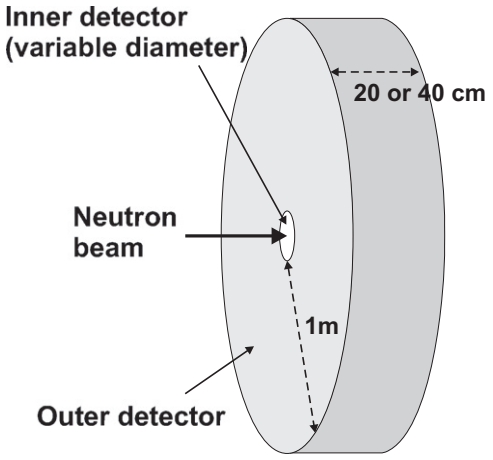

Fig. 9. Setup used in the evaluation of the probability that one neutron generates a signal in more than one detector module.

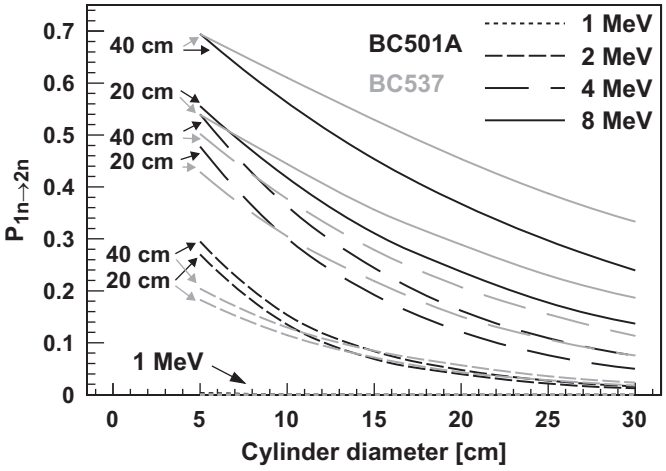

Fig. 10. The probability to have an interaction in two detector modules ($P_{1n\to 2n}$) as a function of the cylinder diameter. Four sets of lines, corresponding to neutron energies 1, 2, 4 and 8 MeV, are shown for each of the two scintillators, BC501A and BC537 in black and grey, respectively. Cylinders with two lengths, 20 and 40 cm, were used and the respective lines are marked with text labels and arrows.

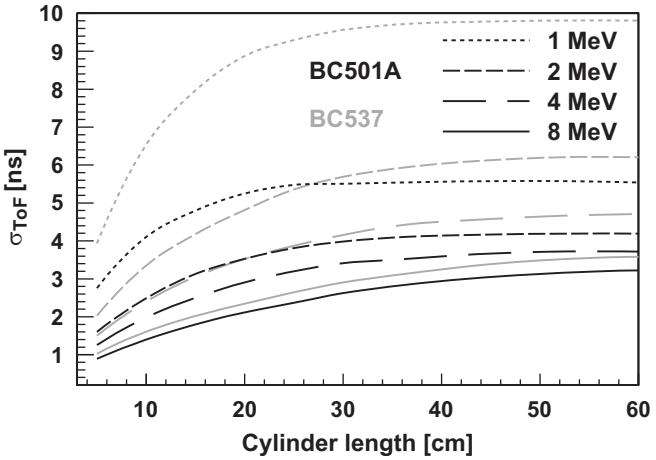

Fig. 11. Width (one standard deviation) of the time-of-flight distributions as a function of the cylinder length for BC501A (black lines) and BC537 (grey lines), and for 1, 2, 4 and 8 MeV neutrons.

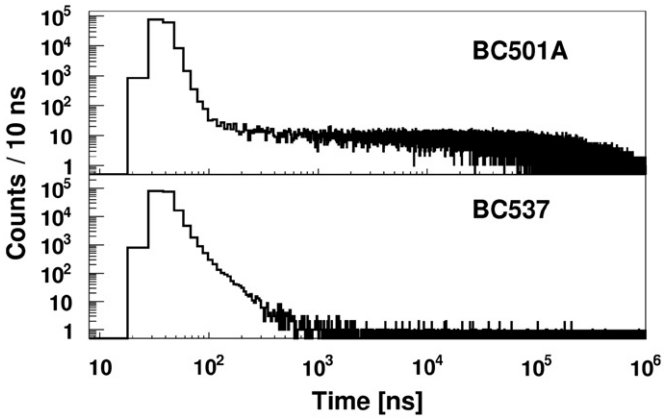

Fig. 12. Times of the significant interaction in the outer detector of the two scintillators shown in Fig. 9. A source of 2 MeV neutrons was placed 51 cm in front of the detectors and the time measurement starts when a neutron is emitted from the source. The detectors were 20 cm long and the diameter of the inner detector was 12.7 cm.

size, as the time-of-flight parameter is used to distinguish neutrons and γ rays detected in the scintillator as well as for the 1n/2n discrimination. Two different components contribute to the time resolution of a neutron detector:

- intrinsic time resolution, related to the time required to produce and collect the light signal in the scintillator, and to the electronic jitter;
- varying time-of-flight due to a distribution of significant interaction depths in a thick detector.

The intrinsic time resolution cannot be evaluated in our simulations, as light production processes and light transportation are not included in the model. It was, however, experimentally shown in Ref. [37] that the intrinsic resolution of BC501A detectors does not significantly vary with the cylindrical detector length. A value of about 1.5 ns was obtained.

The time-of-flight resolution of a cylindrical detector (the same one as described in Section 4) was evaluated as a function of the cylinder length. The widths of the time-of-flight distributions are presented in Fig. 11. Here, the intrinsic time resolution of the detector was not taken into account, and the presented values reflect only the variations of the interaction depths.

The width of the time-of-flight distributions as a function of detector length initially rises rather steeply, while for longer cylinders (above 30 cm) it saturates at a certain value. Thus, our simulations do not indicate any limit on the detector length imposed by the time-of-flight resolution. Larger neutron energies lead to smaller time-of-flight variations, which is due to the fact that for a faster particle, variations in the significant interaction depth are less important in terms of time-of-flight. Filling the detector with the BC537 scintillator liquid, results in a significantly worse time-of-flight resolution than in the case of BC501A.

Timing effects are important for the $P_{1n\to 2n}$ probability. Neutrons interacting in the scintillator usually undergo a series of elastic interactions with the nuclei of the medium and then thermalize or escape from the detector. Thus, light is mostly produced within a few nanoseconds after the neutron enters the detector. Scattering of thermilized neutrons in the scintillator may, however, continue for much longer times (up to milliseconds). If a thermilized neutron is captured by a proton, this leads to a very late light flash, due to the registration of the γ ray emitted in this process. Such effects are more significant for the BC501A scintillator than for BC537, because the cross-section for the p(n, γ)d interaction is much larger than for d(n, γ)t. This is illustrated in Fig. 12, which shows times of the interaction in the

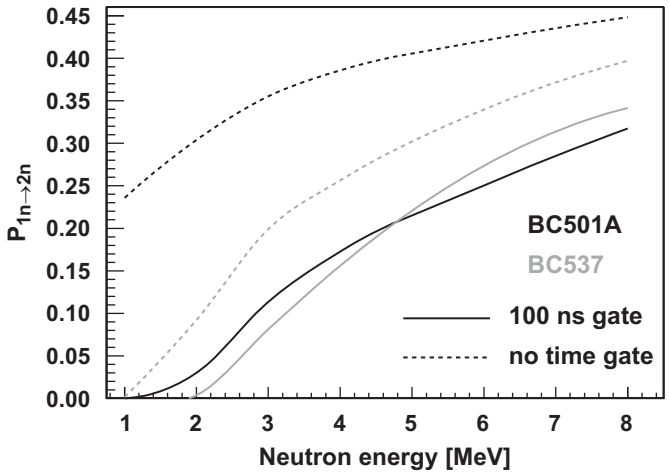

Fig. 13. Influence of the 100 ns detection time limit on the $P_{1n\to 2n}$ probability.

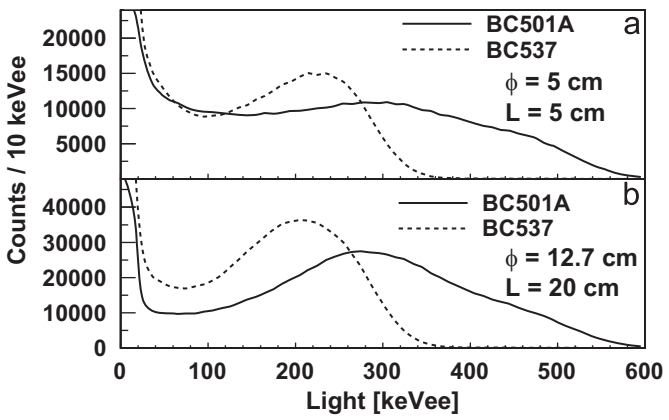

Fig. 14. Light produced by a pencil beam of 2 MeV neutrons in two cylindrical BC501A and BC537 detectors of different size: (a) a small and (b) a large detector. The dimensions of the detectors are shown in the legends.

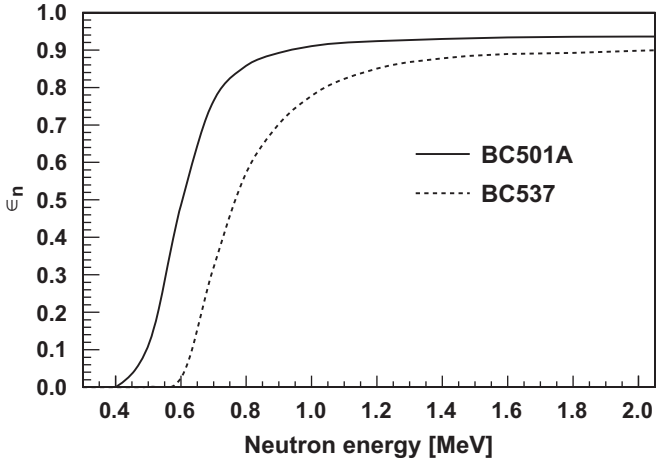

Fig. 15. Neutron detection efficiency as a function of neutron energy for the two scintillators BC501A and BC537. The detector had a diameter of 50 cm and was 60 cm long.

outer detector of the setup shown in Fig. 9. Indeed, for BC501A, a significant interaction in the outer detector either happens within the first 100 ns, or much later, with an almost flat distribution up to hundreds of μs. The corresponding spectrum for the BC537 scintillator shows no such late light-flash effect.

The late light flash is often produced far from the initial neutron interaction point, i.e. usually in another detector module. Thus, the BC501A scintillator seemingly shows much larger $P_{1n\to 2n}$ values than BC537, if light collection is not limited in time. This is illustrated in Fig. 13 in which $P_{1n\to 2n}$ values of the two scintillators are compared for calculations with and without a 100 ns time limit for the significant interaction. This indicates the importance of properly setting time limits on the collection of neutron signals, both in experiments and in simulations. For the efficiency and $P_{1n\to 2n}$ evaluations presented in this paper, a time limit of 100 ns from the emission of neutrons or γ rays to the first significant interaction was used. Light produced in each detector volume was integrated during 300 ns after the significant interaction.

7. Comparison of the two scintillators

As mentioned before, the elsewhere reported advantage of the deuterated scintillator (BC537) is its ability to give a better detector response, i.e. signals which are more proportional to the energy of the incoming neutron, than scintillators based on ^{1}H (like BC501A). Fig. 14 shows simulated light spectra produced by a pencil beam of 2 MeV neutrons interacting in two cylindrical detectors filled with BC501A and BC537, of two different sizes: a small detector with a 5 cm diameter, a 5 cm length and a volume of 0.1 l and a large one with a diameter of 12.7 cm, a length of 20 cm and a volume of 2.5 l. The large detector has a size that likely will be similar to the size of the NEDA detector module. It can be seen in Fig. 14a that the small BC537 detector indeed gives a pronounced bump corresponding to the incident neutron energy. This bump is not seen in the histogram of the small BC501A detector. However, in the big detector (Fig. 14b), events in which most of the neutron energy is transferred to the scintillator medium in one interaction are relatively rare, and no advantage related to the angular distributions of a single neutron scattering can be observed. Instead, events with multiple neutron interactions dominate, leading to very similar shapes of the spectra for both scintillators. The main difference is that less light is produced in BC537 than in BC501A.

It has already been shown (Fig. 6) that the BC537 scintillator has a lower efficiency than BC501A. The difference between the two scintillators is additionally illustrated in Fig. 15 in which the detection probability for the cylindrical detector is plotted as a function of neutron energy. Note that at low neutron energies, below 1 MeV, the efficiency difference between the two scintillators is very significant.

It should be pointed out that the observed difference between the two scintillators comes mainly from the higher cross-section for the neutron interaction with protons than with deuterons. In addition, there is relatively more carbon in BC537 (C_6D_6) than in BC501A (C_8H_{10}) and interactions on carbon give very little light. Also, less light is produced per MeV by deuterons than by protons. Thus, the results of the simulations are easily explained by the physical properties of the scintillation material. A smaller amount of light also results in broader time of flight distributions. As far as the $P_{1n\to 2n}$ probability is concerned, both detectors exhibit similar behaviour, except for the situations when the efficiency of BC537 is too low to register two significant interactions. We conclude that based on the simulations we see no advantage of using the deuterated scintillator instead of the standard one. This conclusion should, however, be verified by experimental tests of the two scintillators. Such tests have already been initiated by the NEDA collaboration and the results will be presented in forthcoming publications.

8. Summary and conclusions

The evaluation of the reliability of the Geant4 neutron interaction model leads to the conclusion that this code can be used for NEDA type simulations, although deficiencies of inelastic processes on ^{12}C and ^{2}H can still be identified. The credibility of the Geant4 neutron interaction model was concluded after comparing the results of simulations with real detector measurements.

Based on the calculations presented in this work, we conclude that a 20 cm deep detector is sufficient for detection of neutrons typically emitted in fusion-evaporation reactions, i.e. for neutrons with energies up to 10 MeV, with the maximum of the energy distribution between 2 and 3 MeV. A longer detector would give only a marginal increase of the efficiency, with a larger probability for a single neutron to generate signals in more than one detector and a possibly worse neutron–γ discrimination capability.

A significant fraction of detected neutrons will create a second signal in detectors situated far away from the initial interaction point. Thus, there is little profit in using detectors of the small transverse dimension (diameter). Note that the NEDA array will likely be situated about 1 m from the neutron emission point (a target) and will cover 1–2π solid angle. A small transverse dimension would then lead to a huge number of the detector modules, which should be avoided, if it is not especially justified. Therefore, we conclude that the diameter of the detector should be as large as practically possible, and this means using detectors of about 5 in. diameter, which is the size of the largest photomultiplier tubes commonly available. An array covering 2π of the solid angle, situated 1 m away from the target will consist of about 400 such detectors.

Our simulations indicate no advantage of using a deuterated scintillator instead of the standard ^{1}H-based one.

Acknowledgements

This work was partly supported by the Polish Ministry of Science and Higher Education, grant no. N N202 073935, by the Swedish Research Council, by the European Union within the Spiral2 Preparatory Phase project (7t Framework Programme, project no. 212692), by the LEA COPIGAL and COPIN-IN2P3 collaborations, and within the framework of the European Social Fund through the Warsaw University of Technology Development Programme, realised by the Center for Advanced Studies. A. Gadea and E. Farnea acknowledge the support of MICINN, Spain, and INFN, Italy, through the AIC10-D-000568 bilateral action. A. Gadea and T. Hüyük have been partially supported by the MICINN and Generalitat Valenciana, Spain, under grants FPA2008-06419 and PROMETEO/2010/101. We acknowledge help of colleagues from the National Centre for Nuclear Research at Świerk, Poland, in particular of Ł. Świderski, and thank them for providing one of the detectors and electronics. Valuable discussions with J.L. Tain, D. Cano-Ott and A. Algora are also acknowledged.

References

[1] Ö. Skeppstedt, et al., Nuclear Instrumentation and Methods in Physics Research Section A 421 (1999) 531.
[2] J. Ljungvall, M. Palacz, J. Nyberg, Nuclear Instrumentation and Methods in Physics Research Section A 528 (2004) 741.
[3] D.G. Sarantites, et al., Nuclear Instrumentation and Methods in Physics Research Section A 530 (2004) 473.
[4] J. Cederkäll, B. Cederwall, A. Johnson, M. Palacz, Nuclear Instrumentation and Methods in Physics Research Section A 385 (1996) 166.
[5] S. Agostinelli, et al., Nuclear Instrumentation and Methods in Physics Research Section A 506 (2003) 250.
[6] J. Allison, et al., IEEE Transactions on Nuclear Science NS-53 (2006) 270.
[7] Saint Gobain Cristals, USA, BC501/BC501A/BC519, data sheet, 〈http://www.detectors.saint-gobain.com〉.
[8] R.A. Cecil, B.D. Anderson, R. Madey, Nuclear Instrumentation and Methods in Physics Research 161 (1979) 439.
[9] Saint Gobain Cristals, USA, BC537 Data Sheet 〈http://www.detectors.saint-gobain.com〉.
[10] W. Tornow, W. Arnold, J. Herdtweck, G. Mertens, Nuclear Instrumentation and Methods in Physics Research Section A 244 (1986) 477.
[11] D.A. Roberts, et al., IEEE Transactions on Nuclear Science NS-39 (1992) 532.
[12] M. Ojaruega, et al., in: IEEE Nuclear Science Symposium Conference Record N24-164, 2007.
[13] M. Ojaruega, Ph.D. Thesis, University of Michigan, 2009.
[14] Computer code evapOR, N.G. Nicolis, D.G. Sarantites, J.R. Beene, see also 〈ftp://ftp.phy.ornl.gov/pub/evapOR/〉 (unpublished).
[15] S.-T. Park, Journal of Radioanalytical and Nuclear Chemistry 256 (2003) 163.
[16] S. Ahhayoun, et al., Nuclear Instrumentation and Methods in Physics Research Section A 668 (2012) 26.
[17] J. Simpson, et al., Acta Physica Hungarica: Heavy Ion Physica 11 (2000) 159.
[18] C. Ur, LNL Annual Report, 2009, p. 68.
[19] A. Maj, et al., Acta Physica Polonica B 40 (2009) 565.
[20] J.N. Scheurer, Nuclear Instrumentation and Methods in Physics Research Section A 385 (1997) 501.
[21] G. de Angelis, et al, in: H. Grawe (Ed.), Ancillary Detectors and Devices for EUROBALL, GSI Darmstadt, 1998.
[22] M. Palacz, et al., Nuclear Instrumentation and Methods in Physics Research Section A 550 (2005) 414.
[23] E. Farnea, et al., Nuclear Instrumentation and Methods in Physics Research Section A 621 (2010) 331.
[24] Geant 4.9.2 Release Notes, 〈http://geant4.cern.ch/support/ReleaseNotes4.9.2.html.〉.
[25] M.B. Chadwick, et al., Nuclear Data Sheets 107 (2006) 2931.
[26] P.I. Dee, C.W. Gilbert, Proceedings of the Royal Society of London. Series A, Mathematical and Physical Sciences 163 (913) (1937) 265.
[27] W.F. Caplehorn, G.P. Rundle, Proceedings of the Physical Society Section A 64 (1951) 546.
[28] G.F. Knoll, Radiation Detection and Measurement, John Wiley Sons, 1989. (Chapter 15.III).
[29] E. Dekempeneer, H. Liskien, L. Mewissen, F. Poortmans, Nuclear Instrumentation and Methods in Physics Research Section A 256 (1987) 489.
[30] S.E. Arnell, et al., Nuclear Instrumentation and Methods in Physics Research Section A 300 (1991) 303.
[31] N.J. Roberts, L.N. Jones, Radiation Protection Dosimetry 126 (2007) 83.
[32] P. Coelho, et al., Nuclear Instrumentation and Methods in Physics Research Section A 280 (1989) 270.
[33] The NDE202 was built by D.Wolski, M. Moszyński, et al. at The Andrzej Soltan Institute for Nuclear Studies, Swierk, Poland.
[34] F.D. Brooks, Nuclear Instrumentation and Methods in Physics Research 4 (1959) 151.
[35] P.-A. Söderström, et al., Nuclear Instrumentation and Methods in Physics Research Section A 594 (2008) 79.
[36] M. Moszyński, et al., Nuclear Instrumentation and Methods in Physics Research Section A 350 (1994) 226.
[37] K. Banerjee, et al., Nuclear Instrumentation and Methods in Physics Research Section A 608 (2009) 440.